ACS NANO

www.acsnano.org

ARTICLE

Flexible Nanoporous Template for the Design and Development of Reusable Anti-COVID-19 Hydrophobic Face Masks

Nazek El-Atab, Nadeem Qaiser, Huda Badghaish, Sohail F. Shaikh, and Muhammad Mustafa Hussain*

Cite This: *ACS Nano* 2020, 14, 7659−7665

Read Online

ACCESS | Metrics & More | Article Recommendations | Supporting Information

ABSTRACT: **Since the outbreak of the severe respiratory disease caused by the novel coronavirus (COVID-19), the use of face masks has become ubiquitous worldwide to control the rapid spread of this pandemic. As a result, the world is currently facing a face mask shortage, and some countries have placed limits on the number of masks that can be bought by each person. Although the surgical grade N95 mask provides the highest level of protection currently available, its filtration efficiency for sub-300 nm particles is around 85% due to its wider pore size (∼300 nm). Because the COVID-19 virus shows a diameter of around 65−125 nm, there is a need for developing more efficient masks. To overcome these issues, we demonstrate the development of a flexible, nanoporous membrane to achieve a reusable N95 mask with a replaceable membrane and enhanced filtration efficiency. We first developed a flexible nanoporous Si-based template on a silicon-on-insulator wafer using KOH etching and then used the template as a hard mask during a reactive ion etching process to transfer the patterns onto a flexible and lightweight (<0.12 g) polymeric membrane. Pores with sizes down to 5 nm were achieved with a narrow distribution. Theoretical calculations show that airflow rates above 85 L/min are possible through the mask, which confirms its breathability over a wide range of pore sizes, densities, membrane thicknesses, and pressure drops. Finally, the membrane is intrinsically hydrophobic, which contributes to antifouling and self-cleaning as a result of droplets rolling and sliding on the inclined mask area.**

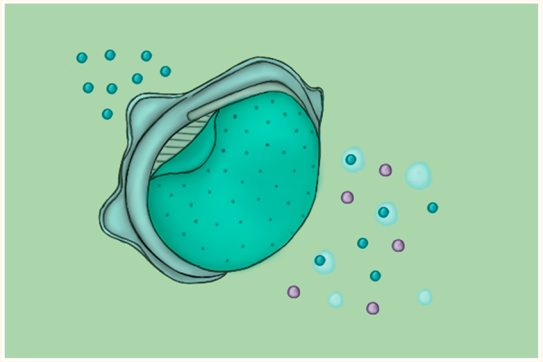

KEYWORDS: *COVID-19, membrane, nanopores, reusable mask, KOH, hydrophobic*

In December 2019, an outbreak of a severe pneumonic disease due to the novel coronavirus (COVID-19) started in Wuhan, China, and then rapidly spread around the world. As of May 9, 2020, the COVID-19 virus has been confirmed in 4,080,426 people worldwide with 279,286 deaths,[1] resulting in a higher mortality rate than influenza. The disease is extremely infectious, with infected people mainly experiencing fatigue, dry cough, and fever, although a large percentage of carriers remain asymptomatic. Virus transmission is believed to take place *via* respiratory droplets resulting from sneezing and coughing.[2−5] Respiratory droplets exist in different sizes,[6,7] where aerosols specifically consist of droplets that are sub-5 μm in size. Droplets that are larger than 5 μm generally do not travel long distances and settle within 1−2 m as a result of gravitational force.[8] However, aerosols are smaller and lighter and therefore can remain floating in the air for extended periods, which can severely increase the spread of the virus.[9−11] Thus, the use of facial masks provides a physical barrier that inhibits exposure to respiratory droplets.[12−14]

Unprecedented measures have been taken globally to stop the rapid spread of this ongoing pandemic, including travel restrictions, remote working, and homeschooling. Moreover, wearing masks when going out in public became necessary and obligatory in some regions to reduce the transmission and contamination rate. As a result, demand for single-use surgical masks escalated drastically. The sudden increase in the demand for such face masks led to their shortage in the market and the inability of the manufacturers to ramp up their capacity to meet the demands. Consequently, several countries have placed limitations on the maximum number of masks a person can buy

Received: May 12, 2020
Accepted: May 20, 2020
Published: May 20, 2020

https://dx.doi.org/10.1021/acsnano.0c03976
ACS Nano 2020, 14, 7659−7665

during a specific period. For instance, in Taiwan, a person can purchase no more than 2 masks per week.[15] In addition, it was suggested that the protective masks should be reserved for workers in the health sector who are at higher risk.[16]

Although several types of commercial face masks can provide different levels of protection, the surgical grade N95 is found to be the most efficient mask so far.[17] However, it is expensive, in limited supply, and its filtration efficiency for particles with sizes smaller than 300 nm is around 85% due to the larger pore size in the filter layer (~300 nm).[17] Moreover, the COVID-19 virus has been shown to belong to the beta-COVs category with an elliptic or spherical shape and size in the range of 65−125 nm,[18] which confirms the need for the development of more efficient filtration masks. In general, air filters can be divided into two main categories: depth filters and membranes.[19] Depth filters are usually based on cellulose, glass fibers, or glass wool, and the filtering mechanism is based on either impaction, interception, diffusion, sedimentation, or electrostatic attraction.[19] Depth filters achieve air stabilization by retaining the particles within them rather than on their surface. In contrast, membrane-based filters consist of a thin and porous polymeric film, and the filtration mechanism is based on straining.[19] In this case, the size of the pores is smaller than the size of the particles, causing their filtration. Nevertheless, one issue that arises in such filters is cake formation in which filtered particles accumulate on the surface of the membrane and then block and limit the passage of additional filtrate through the membrane. As a result, an antifouling mechanism is needed to clean the filter in this case.

To overcome the above-mentioned problems, we demonstrate the development of a nanoporous membrane (down to 5 nm pores) that can be attached on a reusable N95 mask and replaced after every use. The porous membrane is based on a naturally hydrophobic polymer such that the droplets that come into contact with the mask will roll and slide over the mask due to the large inclination angle of the membrane when worn on the face mask. The membrane is developed by first fabricating a Si-based nanoporous template *via* patterning and potassium hydroxide (KOH) etching of a silicon-on-insulator wafer. The released porous template is then used as a hard mask to transfer the patterns onto an ultrathin and hydrophobic polymeric film *via* reactive ion etching (RIE). The porous template can be reused to develop multiple membranes; in addition, the template can be reused on the same membrane following a "step-and-repeat" process to increase its porosity. The results show that nanopores with sizes down to 5 nm can be achieved with a narrow distribution. We performed theoretical calculations to assess the breathability of the obtained membrane and found that airflow rates above 85 L/min can be obtained. Finally, we analyzed the effects of the pore size, density, membrane thickness, and pressure drop on the breathability of the mask. Thus, the proposed solution is to develop nanoporous membranes that could be attached on top of an N95 mask to provide protection against the COVID-19 virus. After every use, the membrane would be removed and replaced with a new one while the same N-95 mask would be reused, as explained in Figure 1.

To develop the membrane, a Si-based porous template is first fabricated. An SOI wafer with 77 nm thick active silicon coated with a 15 nm thick SiO_2 hard mask is initially patterned using e-beam lithography such that an array of 90 nm by 90 nm squares is obtained. The spacing is initially fixed at 200 nm to avoid the proximity effect. Next, RIE is used to get rid of the SiO_2 hard mask in the exposed areas, whereas KOH is used to achieve V-grooves. KOH etches Si preferentially in the ⟨100⟩ plane, leaving behind V-grooves with sidewalls that form at 54.7° with the surface. The final size of the apertures/pores is, thus, a function of the patterned square features, the thickness of the SOI, and the KOH etch time. Therefore, photolithography could be used to pattern larger squares (in the micrometer range) when the initial thickness of the SOI is thicker (in the micrometer range). The SOI is then released by etching the BOX layer using vapor HF, as depicted in Figure 2. Finally, the porous template is coated with a sputtered layer of copper to enhance its mechanical resilience and its etch selectivity when used as a hard mask in the development of the membranes.

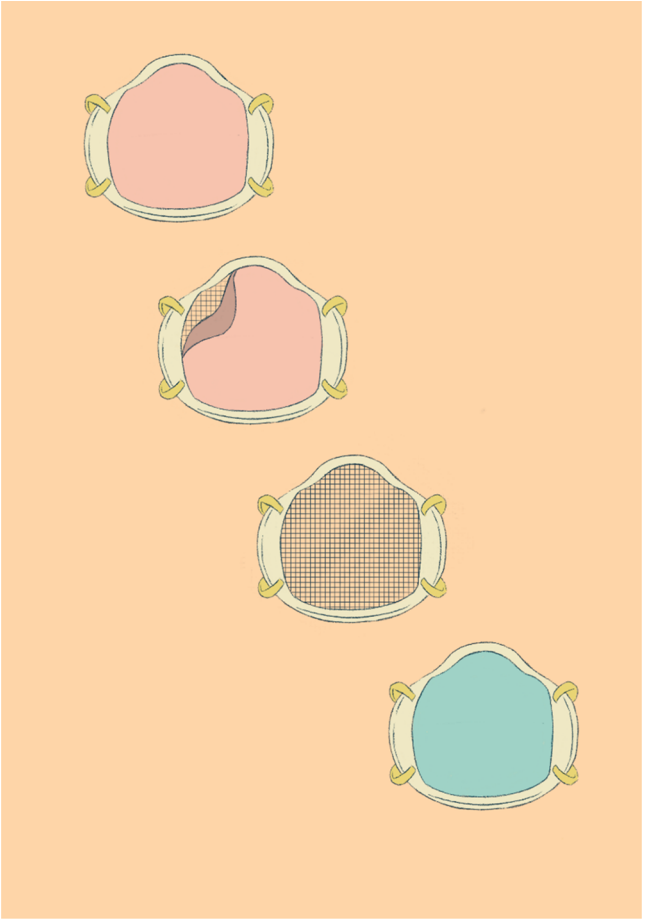

Figure 1. Schematic showing the use of the nanoporous membrane fabricated on an 8 in. wafer on a reusable N95 mask after folding it. The membrane can be replaced after every use.

On another Si(100) wafer with thermally grown SiO_2, a 10 μm polyimide (PI) film is spin-coated and cured. We used the SiO_2 layer because its bonding energy with PI is lower than that with Si, which eases the process of peeling off the membrane. The template with nanopores would then be physically secured on top of the PI film and employed as a hard mask during the PI plasma etching in an RIE system in order to transfer the nanopatterns onto the polymeric film. Finally, the hard mask is removed while the nanoporous membrane is peeled off; the membrane can then be attached onto an N95 mask. The PI-based membrane with the same size as the N95 mask is ultralightweight (<0.12 g). Figure 3 depicts the fabrication process flow of the membrane in addition to an optical image of the membrane (Figure S2). It is worth noting that the processes

https://dx.doi.org/10.1021/acsnano.0c03976
ACS Nano 2020, 14, 7659−7665

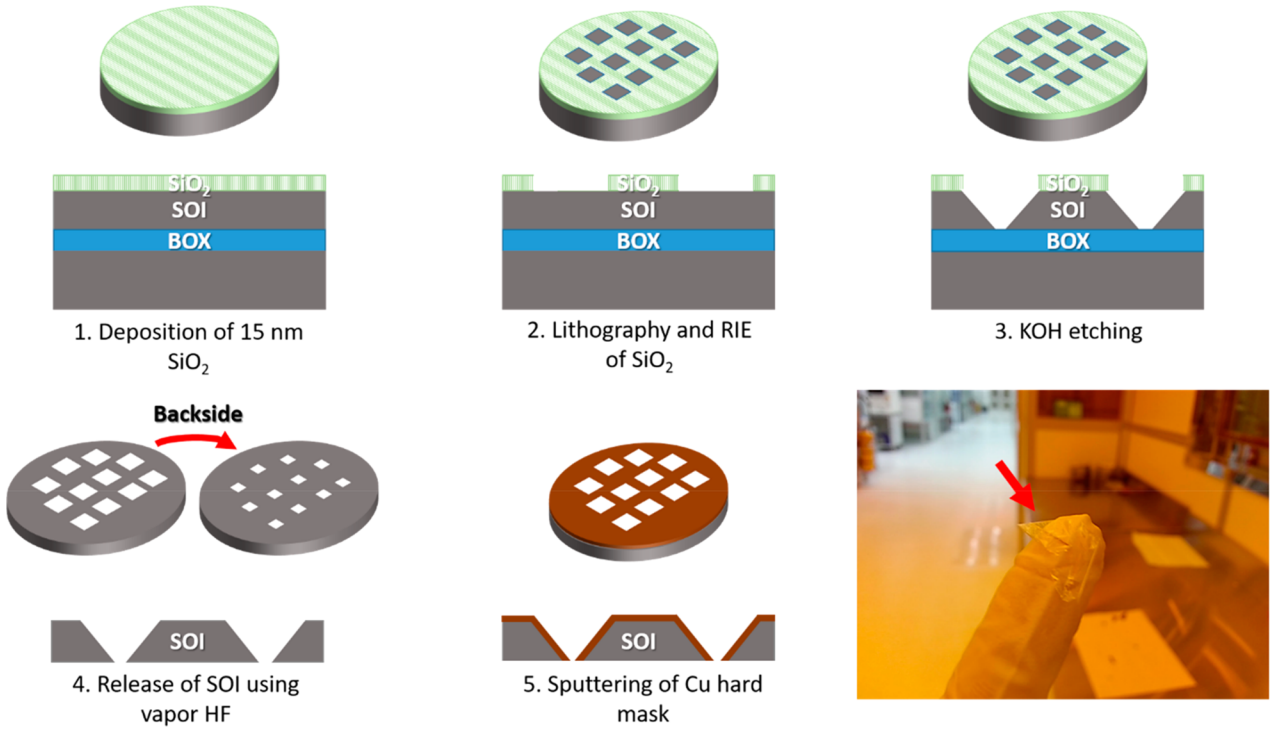

Figure 2. Fabrication process flow of the Si-based nanoporous template using a combination of patterning and KOH etching to achieve the nanosized pores. Optical image of the flexible SOI is shown.

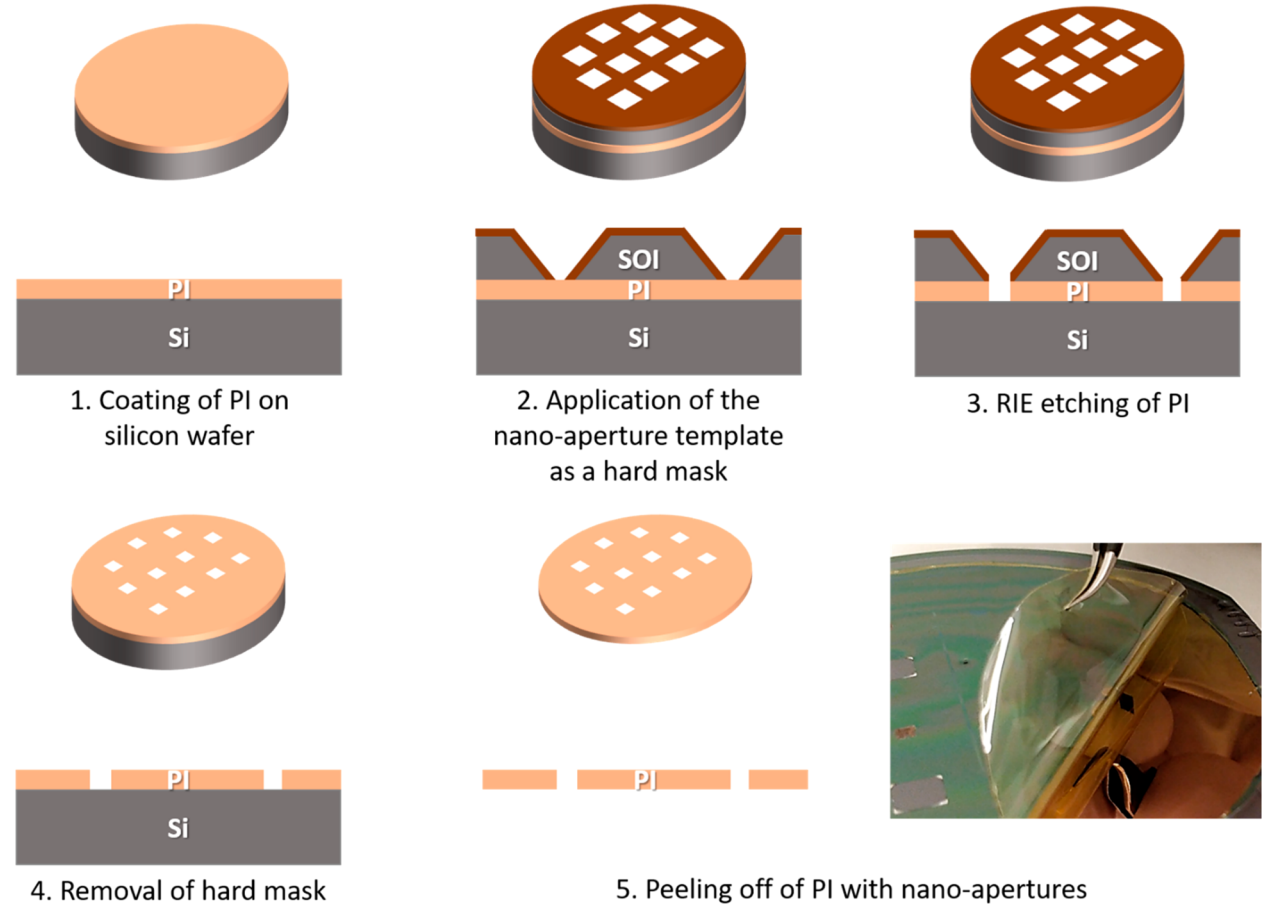

Figure 3. Fabrication process flow of the flexible hydrophobic membrane based on a polyimide thin film with nanopores.

https://dx.doi.org/10.1021/acsnano.0c03976
ACS Nano 2020, 14, 7659−7665

of coating/curing and etching of such a PI-based layer using RIE has been previously demonstrated by our group.[20,21]

RESULTS AND DISCUSSION

We characterized the obtained pore sizes after etching in KOH for different durations using scanning electron microscopy (SEM), as shown in Figure 4. The size of the square apertures

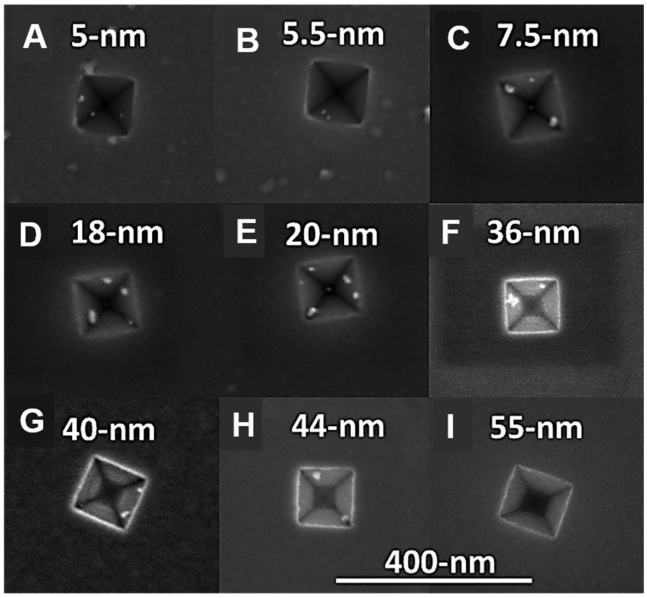

Figure 4. Scanning electron microscopy images of the nanoapertures after etching in 44% KOH at 72 °C for (A) 12 s, (B) 12 s, (C) 12 s, (D) 15 s, (E) 16 s, (F) 19 s, (G) 20 s, (H) 21 s, and (I) 23 s. The patterned 90 nm by 90 nm squares are also visible in the SEM images.

ranges from 5 nm to 55 nm when the etching time is fixed at 12 s up to 23 s, respectively. The top patterned 90 nm by 90 nm squares are also visible in the SEM images.

The distribution of the pore sizes is narrow (~5 nm), which makes it efficient in the application as a hard mask during membrane development (Figure 5A). We used e-beam lithography in this case to pattern the 90 nm by 90 nm squares due to the thin 77 nm SOI wafer; however, larger patterns could be realized using photolithography when a thicker SOI wafer is available (Figure 5B). Moreover, in this case, the spacing between the nanopores is larger than the spacing between the patterned squares as a result of the etching profile following V-grooves. With a 200 nm spacing between the 90 nm by 90 nm patterned squares, the resulting spacing between 10 nm pores is 280 nm, whereas the resulting spacing between 50 nm pores is 240 nm. Nevertheless, the density of pores or porosity of the membrane can be improved by performing multiple patterning steps with the hard mask using a step-and-repeat process.

Several aerosol filtration mechanisms exist, including gravity sedimentation, interception, impingement, diffusion, and electrostatic attraction.[22,23] Generally, large droplets having dimensions in the range of 1−10 μm experience gravity sedimentation or impingement. For smaller droplets (aerosols), the electrostatic attraction becomes the most efficient filtering mechanism, where charged fibers attract the fine particles and get attached to them.[24] Nevertheless, these mechanisms take place in depth filters consisting of a mesh of fibers where the pore sizes are always larger than the fine particle sizes. Thus, air velocity plays a key role in the efficiency of the filter, with higher velocities reducing the filtration efficiency. However, the proposed filter is based on a membrane where the main filtering mechanism is straining. In this case, filtration occurs because the size of the pores is smaller than the size of the particles, so the efficiency of the filter does not depend on the air velocity. Therefore, it is necessary to customize the pore dimensions based on the particles to be removed; for instance, the pore size should be below 60 nm if the droplet containing the COVID-19 virus has a size >60 nm.

Even though the filtration efficiency of straining-based membranes is not affected by the airflow rate through it, the airflow rate does have a great impact on the breathability of the mask. According to the United States National Institute for Occupational Safety and Health (NIOSH), the airflow rate through a mask should be >85 L/min, which corresponds to a moderately high work rate.[25] In addition, according to NIOSH, a certified N95 mask should not show a pressure drop above 343.2 Pa during inhalation and 245.1 Pa during exhalation when tested using an airflow rate of 85 L/min. A higher pressure drop means that a higher airflow resistance would be experienced, which degrades the breathability of the mask. Therefore, in order to assess the performance of the membrane, we calculated the

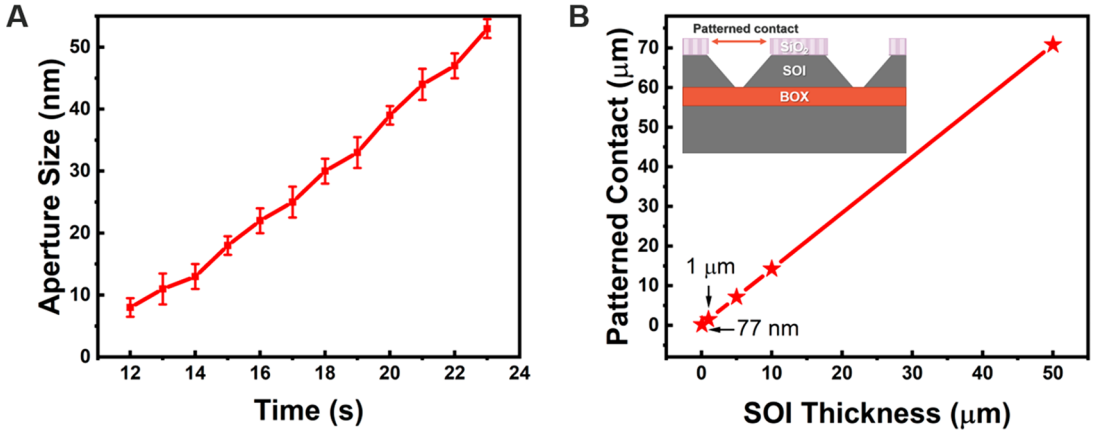

Figure 5. (A) Measured nanoaperture sizes for different etch durations in 44% KOH; the error bar is based on measurements taken on 15 nanoapertures distributed over an area of 5 mm by 5 mm. (B) SOI thickness and corresponding size of the patterned contact to achieve a 100 nm aperture after KOH etching.

https://dx.doi.org/10.1021/acsnano.0c03976
ACS Nano 2020, 14, 7659−7665

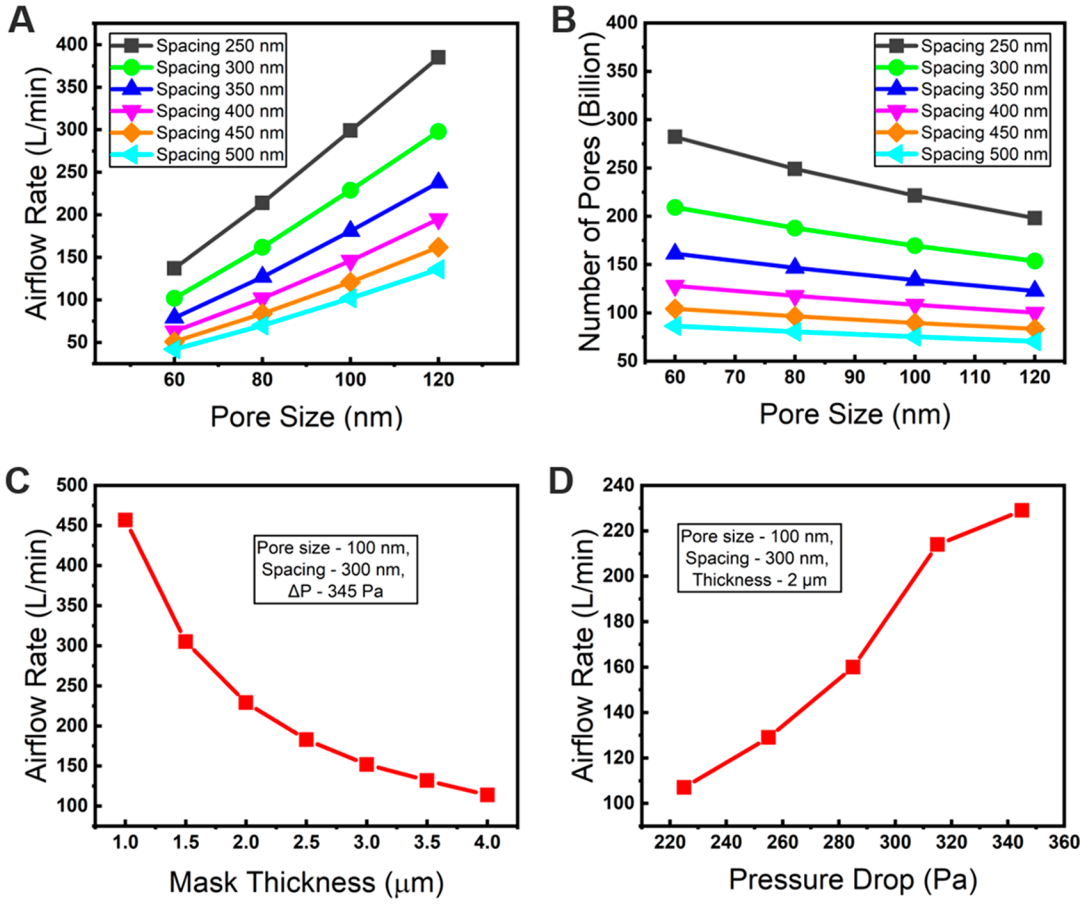

Figure 6. Performance of the nanoporous membrane. (A) Calculated airflow rate through the mask with different pore sizes and densities. The thickness of the mask is fixed at 2 μm, and the ΔP is fixed at 345 Pa. (B) Calculated number of pores in the mask assuming a single patterning step. (C) Calculated airflow rate through the mask for different polyimide thicknesses. (D) Calculated airflow rate through the mask for different pressure drops.

airflow rate through the pores assuming a maximum pressure drop of 345 Pa.[25] We also analyzed the effects of the pores size, density, membrane thickness, and pressure drop on the airflow rate. To simply the calculation, we assumed the shape of the pore to be circular because the pore size is in the nanoscale range. Moreover, we assumed the flow to be laminar with negligible effects of friction. We estimated the air mean velocity U_m using eq 1 and extracted the airflow rate Q using eq 2:

$$U_m = \frac{\Delta P d_p^2}{32 h \eta} \quad (1)$$

$$Q = mAU_m \quad (2)$$

where U_m is the air mean velocity (m/s), d_p is the pore diameter (m), ΔP is the pressure gradient across the mask (Pa), h is the pore length (m), η is the dynamic viscosity of air (Pa·s), m is the number of pores, A is the area of the mask (m^2), and Q is the volumetric flow rate of air through the pores (m^3/s).[26]

The results show that as the size of the pores is increased for the same spacing or when the spacing between the pores is reduced, the airflow rate is increased, meaning that the breathability of the membrane is enhanced due to the enhanced porosity of the membrane (Figure 6A). It is also worth noting that for pores with a size of 60 nm (smaller than the size of the COVID-19), a maximum spacing of ~330 is needed to achieve good breathability (85 L/min). This spacing is possible using state-of-the-art lithography tools based on EUV and DUV. However, when using cheaper proximity photolithography tools, which have a resolution of ~1 μm, multiple patterning of the membrane would be necessary to increase its porosity (Figure 6B). If the patterned squares on the Si template are 1 μm by 1 μm, then the spacing between the nanopores would be >1 μm. The thickness of the PI-based membrane can also be customized by spin-coating it at a higher speed to achieve a thinner membrane with enhanced breathability (Figure 6C). In addition, the membrane enables breathability across a wide range of pressure drops (Figure 6D). In all of these cases, an increased airflow rate does not affect the filtration efficiency if the membrane pore size is smaller than the COVD-19 size as a result of the straining mechanism.[27] When the pore size of the filter is larger than the particle size (as in the case of an N95 mask with 300 nm pores), then an increased air flow rate has been shown to reduce the filtration efficiency.[28]

Because the main filtration mechanism in the proposed membrane is based on straining, in which particles that are larger than the pore dimensions are filtered, a layer of particles would accumulate on the surface of the membrane, blocking some pores and, therefore, reducing the airflow rate through the membrane, especially if worn for extended durations. As a result, an antifouling mechanism would normally be needed to clean the surface of the membrane. The proposed membrane is based on PI, which is intrinsically hydrophobic (water contact angle >90°).[29,30] When the membrane is worn on the mask, a large

https://dx.doi.org/10.1021/acsnano.0c03976
ACS Nano 2020, 14, 7659−7665

inclination angle is obtained (the membrane is almost vertical), which leads to the rolling and/or sliding off of droplets/aerosols. The rolling of droplets on inclined hydrophobic surfaces has been studied extensively in the past, both experimentally and using simulations, for applications in self-cleaning. As the inclination angle is increased and the droplet size is reduced, the rotational speed of the droplet increases, making the antifouling process faster.[31−33] Finally, the hydrophobicity of PI might be useful in repelling water droplets, which are the carriers of the novel coronavirus.

In conclusion, we demonstrated the development of a Si-based nanoporous template using a combination of lithography and KOH-based isotropic etching steps. Pores with sizes down to 5 nm were achieved with a narrow distribution. The template was then used as a hard mask during the pattern-transfer process onto a polymeric thin film in an RIE system. The flexible membrane could be used on a reusable N95 mask to enhance its filtering efficiency against sub-300 nm particles, including the COVID-19 virus. Moreover, the reusability of the N95 mask contributes toward relieving the challenges arising from the shortage of single-use face masks. The filtration mechanism is based on straining, with pores that are smaller than the virus particles. Theoretical calculations on the airflow rate show that the membrane is breathable over a wide range of pore sizes, densities, membrane thicknesses, and pressure drops. Multiple patterning steps can be performed on the membrane to increase its porosity and to increase the allowable airflow rate through it without affecting its filtration efficiency. Finally, the membrane is based on a naturally hydrophobic polymer which contributes to self-cleaning as a result of the rolling of the droplets on the inclined surface.

MATERIALS AND METHODS

Development of the Porous Si Template. In this work, the size of the squares is fixed at 90 nm by 90 nm, and the KOH etch time is varied to customize the apertures' sizes. A 15 nm SiO_2 layer deposited in a plasma-enhanced chemical vapor deposition tool is used as the etch mask. The SiO_2 layer is deposited in two runs and annealed for 10 min at 900 °C to densify the thin film and to reduce the probability of holes causing its failure as an etch mask. The 90 nm square features are patterned using an e-beam lithography tool (JEOL). After development of the 70 nm thick 950 PMMA A2 e-beam resist in 1:3 methyl isobutyl ketone/DI water for 40 s, the exposed SiO_2 is etched in an RIE system. Finally, the sample is immersed in 44% KOH at 72 °C to get the V-grooves.

Development of the Nanoporous and Hydrophobic Polyimide Membrane. Polyimide (10 μm, PI 2611 from HD Microsystems) was spin-coated on a Si(100) wafer for 30 s at a speed of 2000 rpm. PI requires several curing stages including soft-baking, intermediate curing, and final curing at various temperatures. Soft-baking is conducted at a temperature of 90 °C for 90 s, whereas intermediate curing is performed at a temperature of 150 °C for a period of 90 s, and the final curing step is performed at a temperature of 300 °C for a duration of 30 min. It should be noted that the temperature should be steadily ramped from 150 °C to reach 300 °C at the rate of 240 °C/h. The PI is etched in an Oxford reactive ion etching tool using O_2 plasma.

Airflow Rate Estimation. In the provided estimations of the airflow rates shown in Figure 6, a single patterning step is assumed. However, multiple pattern-transfer steps can be performed following a step-and-repeat process to reduce the spacing between the pores and, thus, increase the porosity of the membrane and its breathability.

ASSOCIATED CONTENT

Supporting Information

The Supporting Information is available free of charge at https://pubs.acs.org/doi/10.1021/acsnano.0c03976.

Large-scale images of the nanoporous template, 10 μm PI thin film development, and membrane attachment method (PDF)

AUTHOR INFORMATION

Corresponding Author

Muhammad Mustafa Hussain − *MMH Laboratories, Electrical Engineering, Computer Electrical Mathematical Science and Engineering Division, King Abdullah University of Science and Technology (KAUST), Thuwal 23955-6900, Saudi Arabia; EECS, University of California, Berkeley, California 94720, United States;* orcid.org/0000-0003-3279-0441; Phone: +966-544-700-072; Email: muhammad.hussain@kaust.edu.sa, mmhussain@berkeley.edu

Authors

Nazek El-Atab − *MMH Laboratories, Electrical Engineering, Computer Electrical Mathematical Science and Engineering Division, King Abdullah University of Science and Technology (KAUST), Thuwal 23955-6900, Saudi Arabia*

Nadeem Qaiser − *MMH Laboratories, Electrical Engineering, Computer Electrical Mathematical Science and Engineering Division, King Abdullah University of Science and Technology (KAUST), Thuwal 23955-6900, Saudi Arabia*

Huda Badghaish − *MMH Laboratories, Electrical Engineering, Computer Electrical Mathematical Science and Engineering Division, King Abdullah University of Science and Technology (KAUST), Thuwal 23955-6900, Saudi Arabia*

Sohail F. Shaikh − *MMH Laboratories, Electrical Engineering, Computer Electrical Mathematical Science and Engineering Division, King Abdullah University of Science and Technology (KAUST), Thuwal 23955-6900, Saudi Arabia*

Complete contact information is available at: https://pubs.acs.org/10.1021/acsnano.0c03976

Author Contributions

M.M.H. conceived the idea and directed the project. N.E.-A. fabricated and characterized the nanoporous template and analyzed the results. N.Q. assisted in the theoretical calculation of the airflow rate through the membrane. All authors discussed the results.

Notes

The authors declare no competing financial interest.

ACKNOWLEDGMENTS

This publication is based upon work supported by the King Abdullah University of Science and Technology (KAUST) Office of Sponsored Research (OSR) under Award No. Sensor Innovation Initiative OSR-2015-Sensors-2707 and KAUST-KFUPM Special Initiative OSR-2016-KKI-2880. The authors would like to acknowledge Prof. Aftab Hussain, Prof. Jhonathan Prieto Rojas, and Dr. Galo Torres Sevilla and Maurilio Matracia who have worked on the release of the template.

REFERENCES

(1) Worldometer - Real Time World Statistics; https://www.worldometers.info/ (accessed 2020-05-09).

(2) Lai, C.; Shih, T.; Ko, W.; Tang, H.; Hsueh, P. Severe Acute Respiratory Syndrome Coronavirus 2 (SARS-Cov-2) and Coronavirus Disease-2019 (COVID-19): The Epidemic and the Challenges. *Int. J. Antimicrob. Agents* **2020**, *55*, 105924.
(3) Wang, J.; Du, G. COVID-19 May Transmit Through Aerosol. *Ir. J. Med. Sci.* **2020**, 1−2.
(4) Workman, A.; Welling, D.; Carter, B.; Curry, W.; Holbrook, E.; Gray, S.; Scangas, G.; Bleier, B. Endonasal Instrumentation and Aerosolization Risk in the Era of COVID-19: Simulation, Literature Review, and Proposed Mitigation Strategies. *Int. Forum Allergy Rhinol.* **2020**, DOI: 10.1002/alr.22577.
(5) Cook, T. Personal Protective Equipment During the Coronavirus Disease (COVID) 2019 Pandemic − A Narrative Review. *Anaesthesia* **2020**, DOI: 10.1111/anae.15071.
(6) Zhang, H.; Li, D.; Xie, L.; Xiao, Y. Documentary Research of Human Respiratory Droplet Characteristics. *Procedia Eng.* **2015**, *121*, 1365−1374.
(7) World Health Organization. Annex C - Respiratory Droplets. In *Natural Ventilation for Infection Control in Health-Care Settings*; Atkinson, J., Chartier, Y., Pessoa-Silva, C. L., Jensen, P., Li, Y., Seto, W. H., Eds.; World Health Organization: Geneva, 2009; pp 77−82.
(8) Morawska, L. Droplet Fate in Indoor Environments, or Can We Prevent the Spread of Infection? *Indoor Air* **2006**, *16*, 335−347.
(9) Morawska, L.; Cao, J. Airborne Transmission of SARS-Cov-2: The World Should Face the Reality. *Environ. Int.* **2020**, *139*, 105730.
(10) Wang, J.; Du, G. COVID-19 May Transmit Through Aerosol. *Ir. J. Med. Sci.* **2020**, DOI: 10.1007/s11845-020-02218-2.
(11) Santarpia, J. L.; Rivera, D. N.; Herrera, V.; Morwitzer, M. J.; Creager, H.; Santarpia, G. W.; Crown, K. K.; Brett-Major, D.; Schnaubelt, E.; Broadhurst, M. J.; Lawler, J. V.; Reid, S. P.; Lowe, J. J. Transmission Potential of SARS-CoV-2 in Viral Shedding Observed at the University of Nebraska Medical Center. *MedRxiv* **2020**; https://10.1101/2020.03.23.20039446 (accessed 2020-04-20).
(12) Ching, W.-H.; Leung, M. K. H.; Leung, D. Y. C.; Li, Y.; Yuen, P. L. Reducing Risk of Airborne Transmitted Infection in Hospitals by Use of Hospital Curtains. *Indoor Built Environ.* **2008**, *17*, 252−259.
(13) Lai, A. C. K.; Poon, C. K. M.; Cheung, A. C. T. Effectiveness of Facemasks To Reduce Exposure Hazards for Airborne Infections Among General Populations. *J. R. Soc., Interface* **2012**, *9*, 938−948.
(14) Leung, N. H. L.; Chu, D. K. W.; Shiu, E. Y. C.; Chan, K.-H.; McDevitt, J. J.; Hau, B. J. P.; Yen, H.-L.; Li, Y.; Ip, D. K. M.; Peiris, J.S. M.; Seto, W.-H.; Leung, G. M.; Milton, D. K.; Cowling, B. J. Respiratory Virus Shedding in Exhaled Breath and Efficacy of Face Masks. *Nat. Med.* **2020**, *26*, 676.
(15) Name-Based Rationing System for Purchases of Masks To Be Launched on February 6; Public To Buy Masks with their (NHI) Cards; https://www.cdc.gov.tw/En/Bulletin/Detail/ZlJrIunqRjM49LIBn8p6eA?typeid=158 (accessed 2020-05-09).
(16) Mehta, P.; McAuley, D.; Brown, M.; Sanchez, E.; Tattersall, R.; Manson, J. COVID-19: Consider Cytokine Storm Syndromes and Immunosuppression. *Lancet* **2020**, *395*, 1033−1034.
(17) Konda, A.; Prakash, A.; Moss, G.; Schmoldt, M.; Grant, G.; Guha, S. Aerosol Filtration Efficiency of Common Fabrics Used In Respiratory Cloth Masks. *ACS Nano* **2020**, DOI: 10.1021/acsnano.0c03252.
(18) Batt, C.; Tortorello, M. Risk and Control of Air Contamination. In *Encyclopedia of Food Microbiology*; Batt, C. A., Robinson, R., Eds.; Academic Press: Cambridge, 2014; pp 204−207.
(19) Shereen, M.; Khan, S.; Kazmi, A.; Bashir, N.; Siddique, R. COVID-19 Infection: Origin, Transmission, and Characteristics of Human Coronaviruses. *J. Adv. Res.* **2020**, *24*, 91−98.
(20) Shaikh, S.; Mazo-Mantilla, H.; Qaiser, N.; Khan, S.; Nassar, J.; Geraldi, N.; Duarte, C.; Hussain, M. Environmental Monitoring: Noninvasive Feather Light Wearable Compliant "Marine Skin": Standalone Multisensory System For Deep-Sea Environmental Monitoring. *Small* **2019**, *15*, 1970051.
(21) Nassar, J.; Khan, S.; Velling, S.; Diaz-Gaxiola, A.; Shaikh, S.; Geraldi, N.; Torres Sevilla, G.; Duarte, C.; Hussain, M. Compliant Lightweight Non-Invasive Standalone "Marine Skin" Tagging System. *npj Flexible Electronics* **2018**, *2*, 13.
(22) Hinds, W. C. Filtration. In *Aerosol Technology: Properties, Behavior, and Measurement of Airborne Particles*, 2nd ed.; John Wiley & Sons: New York, 1999; pp 182−205.
(23) Vincent, J. H. Aerosol Sample Applications and Field Studies. In *Aerosol Sampling. Science, Standards, Instrumentation and Applications*; Vincent, J. H., Ed.; John Wiley & Sons: New York, 2007; pp 528−529.
(24) Colbeck, I.; Lazaridis, M. Filtration Mechanisms. In *Aerosol Science: Technology and Applications*, 1st ed.; Colbeck, I., Lazaridis, M., Eds.; John Wiley & Sons: New York, 2014; pp 89−118.
(25) Kim, J.; Roberge, R.; Powell, J.; Shaffer, R.; Ylitalo, C.; Sebastian, J. Pressure Drop of Filtering Face Piece Respirators: How Low Should We Go? *Int. J. Occup. Med. Env.* **2015**, *28*, 71−80.
(26) Hes, L.; Dolezal, I. Testing of Air Permeability of Distant Knitted Fabrics in the Direction of their Plane. *J. Textile Eng. Fashion Technol.* **2017**, *2*, 547−549.
(27) Liu, B.; Zhang, S.; Wang, X.; Yu, J.; Ding, B. Efficient and Reusable Polyamide-56 Nanofiber/Nets Membrane with Bimodal Structures for Air Filtration. *J. Colloid Interface Sci.* **2015**, *457*, 203−211.
(28) Wang, Q.; Bai, Y.; Xie, J.; Jiang, Q.; Qiu, Y. Synthesis and Filtration Properties of Polyimide Nanofiber Membrane/Carbon Woven Fabric Sandwiched Hot Gas Filters for Removal of PM 2.5 Particles. *Powder Technol.* **2016**, *292*, 54−63.
(29) Yilbas, B.; Al-Sharafi, A.; Ali, H.; Al-Aqeeli, N. Dynamics of a Water Droplet on a Hydrophobic Inclined Surface: Influence Of Droplet Size and Surface Inclination Angle on Droplet Rolling. *RSC Adv.* **2017**, *7*, 48806−48818.
(30) Feng, B.; Xu, K.; Huang, A. Synthesis of Graphene Oxide/Polyimide Mixed Matrix Membranes For Desalination. *RSC Adv.* **2017**, *7*, 2211−2217.
(31) Huang, X.; Chen, B.; Mei, M.; Li, H.; Liu, C.; Wei, C. Synthesis and Characterization of Organosoluble, Thermal Stable and Hydrophobic Polyimides Derived from 4-(4-(1-Pyrrolidinyl)Phenyl)-2,6-Bis(4-(4-Aminophenoxy)Phenyl)Pyridine. *Polymers* **2017**, *9*, 484.
(32) Li, Z.; Guo, Z. Bioinspired Surfaces with Wettability for Antifouling Application. *Nanoscale* **2019**, *11*, 22636−22663.
(33) Yang, G.; Terzis, A.; Zarikos, I.; Hassanizadeh, S.; Weigand, B.; Helmig, R. Internal Flow Patterns of a Droplet Pinned to the Hydrophobic Surfaces of a Confined Microchannel Using Micro-PIV and VOF Simulations. *Chem. Eng. J. (Amsterdam, Neth.)* **2019**, *370*, 444−454.

https://dx.doi.org/10.1021/acsnano.0c03976
ACS Nano 2020, 14, 7659−7665